Materials Today Physics 35 (2023) 101116

Contents lists available at ScienceDirect

Materials Today Physics

journal homepage: www.journals.elsevier.com/materials-today-physics

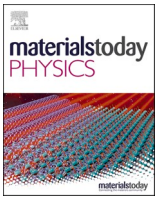

# Magnetic transitions in V-Fe-Co-Ni-Cu-based high entropy alloys

B.G.F. Eggert [a], E.K. Delczeg-Czirjak [b], B.C. Hauback [a], C. Frommen [a,*]

[a] Department for Hydrogen Technology, Institute for Energy Technology (IFE), P.O. Box 40, NO-2027, Kjeller, Norway
[b] Department of Physics and Astronomy, Uppsala University, Box 516, 751 20, Uppsala, Sweden

ARTICLE INFO

*Keywords:*
Magnetocaloric
High entropy alloys
Density functional theory
Microstructure
Scanning electron microscopy

ABSTRACT

FeCoNi, $V_{0.85}$FeCoNi, FeCoNi$Cu_{1.15}$ and $V_{0.85}$FeCoNi$Cu_{1.15}$ alloys have been synthesized by arc melting and analyzed by powder X-ray diffraction, electron microscopy, magnetic measurements, and density functional theory (DFT). The influence of each alloying element on the magnetic exchange interaction, Curie temperature ($T_C$) and magnetocaloric effect is evaluated. The experimental results show that Cu and V "dilute" the magnetic properties and couple antiferromagnetically to Fe, Co, and Ni. Analysis of the microstructure reveals a lack of solubility between V and Cu with FeCoNi, and between themselves, thus lowering the concentration of V and Cu in the main solid solution of the 5-element alloy $V_{0.85}$FeCoNi$Cu_{1.15}$. $T_c$ decreases significantly from 997 K in FeCoNi to 245 K in $V_{0.85}$FeCoNi and 297 K in $V_{0.85}$FeCoNi$Cu_{1.15}$, respectively. The derivative of magnetization as a function of temperature (dM/dT) in the vicinity of $T_c$ is drastically reduced due to the presence of V which indicates a reduced magnetocaloric effect. DFT calculations confirm antiferromagnetic coupling of V to the ferromagnetic FeCoNi-base and predict a similar behavior for other transition metal elements (*e.g.*, Ti, Cr, Mn). This leads to a lowering of $T_c$, which is needed to establish the magnetocaloric effect at room temperature. However, it comes at a cost of reduced magnetic moments. Nevertheless, the use of V and Cu has shown possible routes for tuning the magnetocaloric effect in FeCoNi-based high entropy alloys.

## 1. Introduction

Solid-state magnetocaloric devices aim to deliver more efficient refrigeration with less environmental impact [1,2]. When considering material challenges, high entropy alloys (HEAs) containing 3d metals could meet several of the demands that magnetic heat conversion devices require. They offer corrosion resistance, long-term cyclability, and ease of production, while being produced from abundant, non-expensive materials [3,4]. The core of the magnetocaloric effect (MCE) in these HEAs originates from the use of Fe, Co and Ni, with strong magnetic moments, and magnetic ordering temperatures ($T_C$) of 1043 K (Fe), 1400 K (Co) and 627 K (Ni), respectively.

Since the $T_{C's}$ of the pure elements are far above room temperature (RT), it is necessary to decrease them by alloying Fe, Co, and Ni with other elements [5–8]. This can be achieved by two main approaches: (i) dilution of ferromagnetic exchange interactions via elements such as Cu/Al that induce a zero or close-to-zero exchange interaction with the ferromagnetic transition metals (FMTM), and (ii) use of elements such as Cr, V, Ti etc. that induce antiparallel coupling with the FMTMs. To conveniently bring $T_C$ to RT, both kinds of elements are typically used in FeCoNi-based HEAs [7]. This raises the number of possible magnetic interactions between all elements. Due to an equilibrium between enthalpy and entropy, sub-regular solid solutions are commonly formed. This creates some degree of inhomogeneity or ordering in bulk HEAs [9] that leads to a distribution of $T_C$'s. As a result, the magnetic transition becomes broadened and ultimately results in a reduced MCE. How elements that induce dilution and/or couple antiferromagnetically impact $T_C$ is not well understood, except for Cr and Mn [7,10–13].

In a previous report, we considered V, Al and Cu as alloying elements in $V_{1-x}$FeCoNi$(Al/Cu)_{1+x}$ HEAs [14]. In $V_{0.85}$FeCoNi$Cu_{1.15}$, a multiphasic microstructure was found, that impacted the composition of the main solid solution compared to the nominal composition. The investigation also uncovered an isothermal entropy change ($\Delta S_m$) of 0.17 J/kg.K for a magnetic field change of $\mu_0 H$ = 0–1 T at room temperature in $V_{0.85}$FeCoNi$Cu_{1.15}$, or 0.75 J/Kg.K for $\mu_0 H$ = 0–5 T, which are low values compared to regular magnetocaloric materials [15]. This result is understood as the combined effect of V and Cu in the ferromagnetic transition of FeCoNi. However, since two alloying elements are present, the individual influence of each alloying element on the magnetic transition is not possible to determine.

* Corresponding author.
*E-mail address:* christoph.frommen@ife.no (C. Frommen).

https://doi.org/10.1016/j.mtphys.2023.101116
Received 20 March 2023; Received in revised form 5 May 2023; Accepted 19 May 2023
Available online 20 May 2023

In this article, we investigate how the individual and combined addition of V and Cu affects the (micro)structure and magnetic properties of FeCoNi-based solid solutions. A disordered ferromagnetic FeCoNi base alloy is compared to: (i) a magnetically diluted Cu-doped compound ($FeCoNiCu_{1.15}$), (ii) a V-containing compound ($V_{0.85}FeCoNi$) with ferromagnetic and antiferromagnetic interactions, and (iii) the combined effect of V and Cu in $V_{0.85}FeCoNiCu_{1.15}$, with dilution and antiparallel interactions. This non-equiatomic ratio has been selected as the 5-element alloy displays a magnetic transition around RT [14]. The same ratio is also kept for the respective FeCoNi–Cu and V–FeCoNi 4-element alloys. We pay special attention to the solidification path and metallurgy of the alloys and how they enable an optimized microstructure which is essential for obtaining efficient magnetocaloric materials. The magnetic properties of the alloys are assessed through magnetization measurements, and experimental results are compared to DFT calculations in order to gain better insight into magnetic ordering temperatures, element-resolved magnetic moments, and exchange interactions. Finally, we briefly evaluate by DFT the use of other elements such as Ti, Cr, and Mn to induce antiferromagnetic coupling in FeCoNi-based solid solutions.

## 2. Materials and methods

Metallic powders of Fe, Ni, Co, V, Cu and Al of 99.9% purity were weighed, mixed and arc melted in a Ti-gettered home-built arc melter in argon atmosphere. The samples were remelted and turned 5 times to ensure homogeneity. Nominal compositions are described in Table 1. Powder X-ray diffraction (PXD) was carried out by a Bruker D2 Phaser Cu–K $\alpha$ diffractometer ($\lambda = 1.5406$ Å) in Bragg-Brentano configuration. Rietveld refinements were done using the Fullprof Suite [16]. The presence of stacking faults was modelled by the FAULTS software package, where lattice parameters, crystallite size, and stacking fault probabilities were refined [17]. Scanning electron microscopy (SEM) and energy dispersive X-ray spectroscopy (EDS) were carried out in a Hitachi SU8230 ultra-high-resolution cold-field emission scanning electron microscope used in backscattered electron (BSE) mode. On samples containing the sigma phase, its phase fraction was determined by area analysis using the ImageJ software [18] using three micrographs with 250 times magnification, scanning an area over 0.2 $mm^2$ per image. As the samples show no signs of preferential orientation, it is possible to extrapolate the area percentage to volumetric percentage. Chemical compositions were obtained by area measurements. Magnetic measurements were carried out by a Quantum Design Physical Property Measurement System (PPMS) and a LakeShore Vibrating Sample Magnetometer (VSM). Measurements as a function of temperature were performed in a persistent applied field of $\mu_0$ H = 1 T , and temperatures ranging from 10 to 375 K in the PPMS, and from 300 to 1100 K in the VSM. Field dependent magnetization was performed with applied fields of $\mu_0$H = 0–1 T.

**Table 1**
Atomic concentration of the elements for the nominal compositions of the alloys, together with the compositions for the main ccp solid solutions obtained from EDS measurements.

| Nominal composition (formula units) | Fe (at. %) | Co (at. %) | Ni (at. %) | V (at. %) | Cu (at. %) |
|---|---|---|---|---|---|
| FeCoNi | 33 | 33 | 33 | – | – |
| $FeCoNiCu_{1.15}$ | 24.1 | 24.1 | 24.1 | – | 27.7 |
| $V_{0.85}FeCoNi$ | 26 | 26 | 26 | 22 | – |
| $V_{0.85}FeCoNiCu_{1.15}$ | 20 | 20 | 20 | 17 | 23 |
| main phase composition (formula units) | Fe (at. %) | Co (at. %) | Ni (at. %) | V (at. %) | Cu (at. %) |
| $Fe_1Co_{1.14}Ni_{1.14}$ | 30.5 (30) | 34.8 (3) | 34.7 (3) | – | – |
| $FeCo_{1.16}Ni_{1.09}Cu_{0.84}$ | 24.4 (2) | 28.4 (1) | 26.6 (1) | – | 20.6 (2) |
| $V_{0.82}FeCo_{1.07}Ni_{1.03}$ | 25.4 (2) | 27.4 (3) | 26.3 (1) | 20.9 (4) | – |
| $V_{0.75}FeCo_{1.07}Ni_{1.01}Cu_{0.56}$ | 22.5 (6) | 24.1 (2) | 22.8 (6) | 17.9 (20) | 12.7 (6) |

### 2.1. Theoretical methodology

Phase presence and compositions were predicted by the CALPHAD method implemented in the Thermo-Calc 2021 software in combination with the TCHEA3 high entropy alloy database package. Property diagrams were obtained by considering all the possible phases, including intermetallic and intermediate compounds formed by the constituent elements.

Electronic structure calculations were done by the exact muffin-tin orbital (EMTO) method [19,20] where the chemical and magnetic disorder is treated within the coherent potential approximation (CPA) [21,22] (EMTO-CPA [23]). The electrostatic correction to the single-site CPA was considered as implemented in the Lyngby version of the EMTO code [24]. For details the reader is referred to Refs. [24,25], and [26].

The one-electron Kohn-Sham equations were solved within the soft-core and scalar-relativistic approximations, with $l_{rm\ max} = 3$ for partial waves and $l^{rm\ t}_{rm\ max} = 5$ for their "tails". The Green's function was calculated for 16 complex energy points distributed exponentially on a semi-circular contour including states within 1 Ry below the Fermi level. The exchange-correlation effects were described within the Generalized Gradient Approximation (GGA) in Perdew, Burke, and Ernzerhof (PBE) form [16]. Magnetic exchange interactions were calculated within the magnetic force theorem, implemented in the Lyngby version of the EMTO-CPA [24] code for the ferromagnetic state.

Total energies were calculated within the full-charge density technique [27] using PBE [16] to describe the exchange-correlation effects. For the one-center expansion of the full charge density a cut-off of $l_{\mathrm{rm\ max}} = 8$ was used. $\alpha_i^0 = 0.7$ for the on-site screening constant, and $\beta_{scr} = 1.1$ for the average screening parameter [25,26] was used to account for the contributions of the screened Coulomb interactions to the one-electron potential of the alloy components and the total energy of the system [25,26]. A 12 × 12 x 12 Monkhorst-Pack [28] *k*-mesh grid was used for the Brillouin zone integration. The equilibrium volume (lattice parameter) for the nominal compositions were determined from a Morse [29] equation of state fitted to the *ab initio* total energies of fcc structures for 5 different atomic volumes. Statistical thermodynamics simulations of the magnetic phase transition were done by MC method implemented within the Uppsala atomistic spin dynamics (UppASD) software [30,31]. MC simulations were performed on a 40 × 40 × 40 supercell with periodic boundary conditions. The size and direction of the magnetic moments were chosen randomly at each MC trial and 10000 MC steps were used for equilibration followed by 50000 steps for obtaining thermodynamic averages.

## 3. Results and discussion

### 3.1. Solidification of FeCoNi alloys with V and Cu

FeCoNi-based HEAs are typically ferromagnetic with $T_C$'s in the order of several hundred degrees Kelvin. To tune $T_C$ towards RT, the average exchange interaction needs to be altered by use of other elements. This modifies the liquid and solid solution properties, influencing the morphology of the phases during common (non-equilibrium) solidification processes. To correctly assess the potential of magnetocaloric high entropy alloys, a detailed understanding of the factors that determine phase formation in those materials is essential for tailoring their magnetic properties and microstructure.

Solidification of the FeCoNi parent alloy proceeds without macroscopic segregation, see Fig. 1(a). This indicates a good solubility between the three ferromagnetic elements. The corresponding CALPHAD

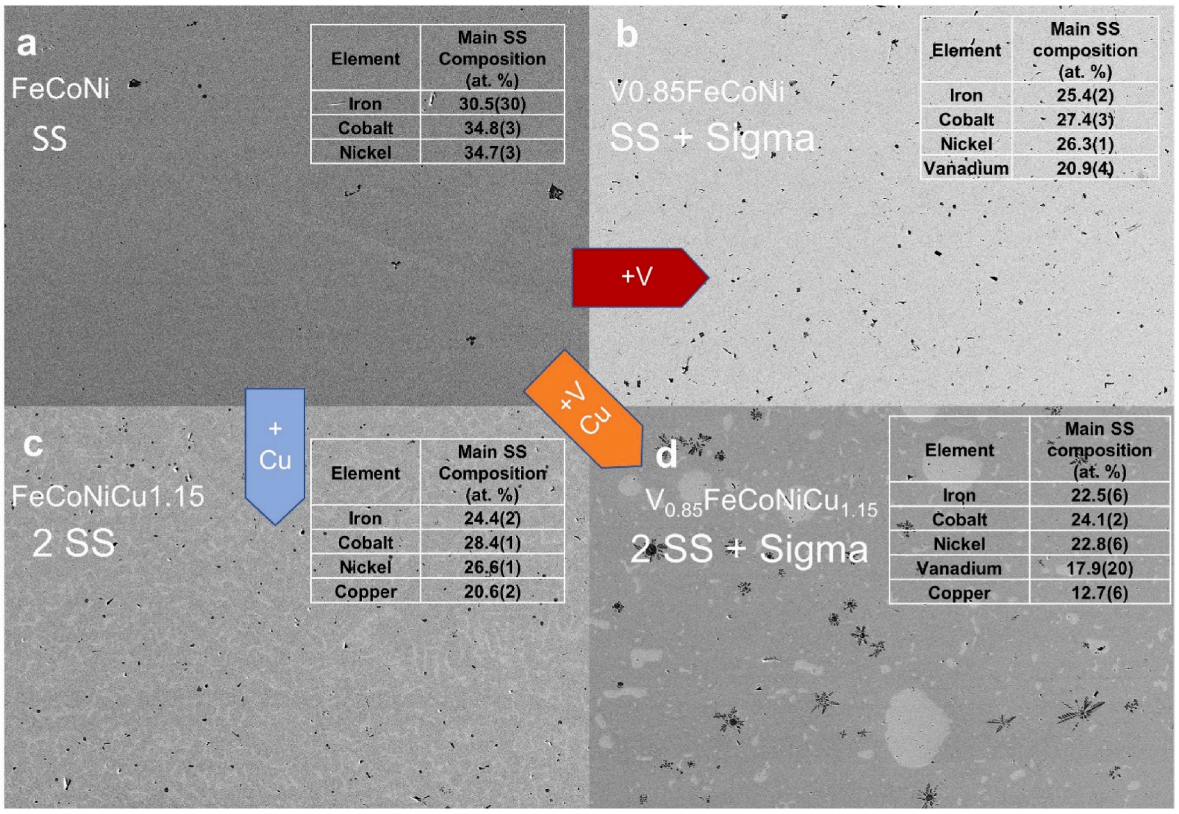


**Fig. 1.** (Color online.) Scanning electron micrographs obtained in BSE mode with a magnification of 250x, showing the microstructure of four solid solutions: (a) FeCoNi, (b) $V_{0.85}$FeCoNi, (c) FeCoNi$Cu_{1.15}$ and (d) $V_{0.85}$FeCoNi$Cu_{1.15}$. Either one or two solid solutions (SS) or a mix of SS and a sigma intermetallic are observed. The atomic composition of the main ccp solid solution is shown in the insert for each of the four studied alloys.

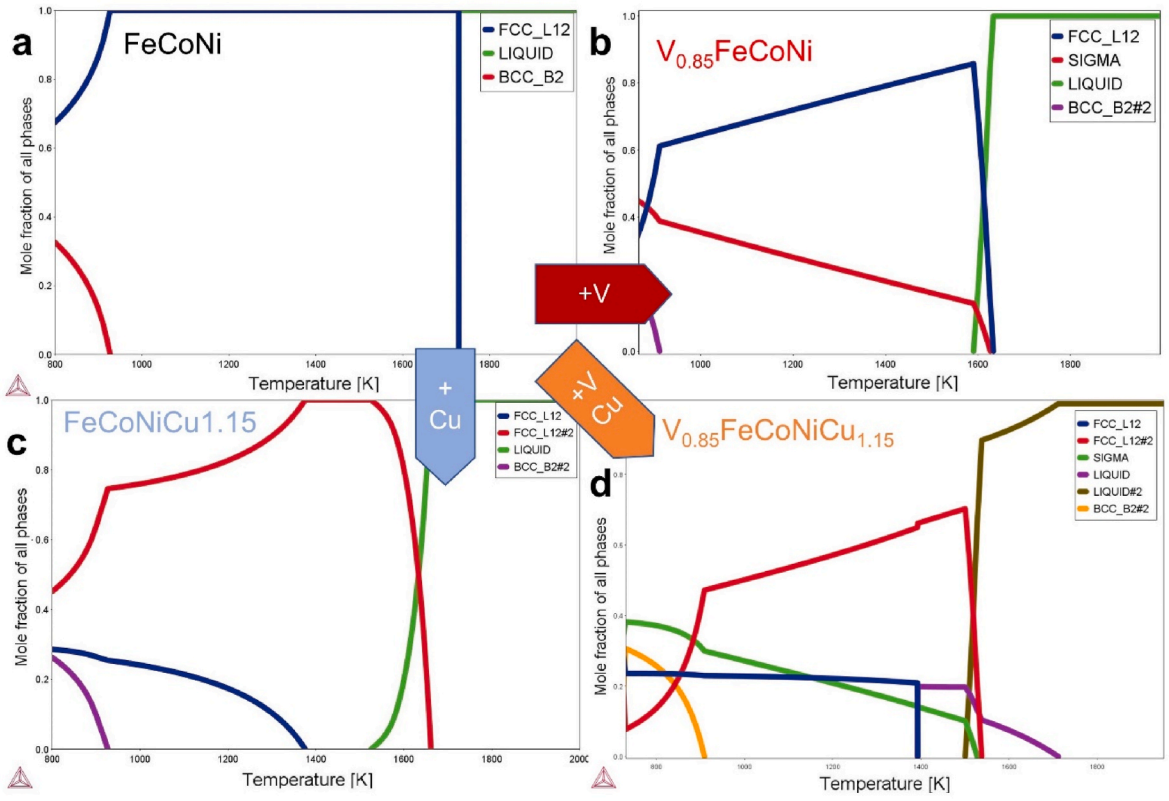


**Fig. 2.** (Color online.) CALPHAD plots indicating the phase presence as a function of temperature for the four studied FeCoNi-based alloys.

plot in Fig. 2(a) predicts the formation of a secondary phase at temperatures below 950 K. Since solidification occurs with a high cooling rate, however, there is not enough thermal activation for the segregation to occur. The addition of V in $V_{0.85}$FeCoNi modifies the solidification process, as is illustrated in the upper-right corner in Fig. 1(b). A sigma phase is present during early stages of sample preparation together with the cubic close-packed (ccp) solid solution (also known as face-centered cubic, space group *Fm*-3*m*); however, it is removed after polishing. The sigma phase is an intermetallic with a tetragonal structure (space group $P4_2/mnm$), and composition $A_2B$, where *A* and *B* are transition metals. The removal can be ascribed to the very different crystal structures, creating incoherence between the ccp structure of the solid solution and the tetragonal structure of the sigma phase [32]. Sigma phases are typically precipitated from solid solutions during heat treatments, but they can also precipitate during solidification. This appears to be the case for the studied V-containing alloys and agrees well with calculated phase fraction plots as a function of temperature obtained by CALPHAD, see Fig. 2(b). By employing image area analysis due to the contrast between the removed phase and the alloy, it is possible to estimate the phase fraction of the sigma phase using ImageJ, with an average value of 0.8% in volume for $V_{0.85}$FeCoNi. Precipitates are seen with a spheroid or polyhedral shape morphology, another indication of the small coherence between the precipitates and the main solid solution. In the V-containing 4-element alloy, displayed in Fig. 1(b), up to 21 at. % V is observed in the main ccp solid solution, together with Fe (25 at. %), Co (27 at. %), and Ni (26 at. %). The chemical compositions of the main solid solutions measured by EDS are shown in the lower section of Table 1.

When Cu is introduced into FeCoNi, as shown in Fig. 1(c), the solubility of Cu in the solid solution decreases as the temperature drops after arc melting. This is confirmed by the CALPHAD prediction for phase presence as a function of temperature in Fig. 2(c), which shows the formation of a secondary ccp phase at temperatures below approximately 1400 K. As a result, dendrites with a composition of $FeCoNiCu_x$ are formed. Once the solubility limit is reached, the remaining Cu solidifies in an inter-dendritic secondary ccp phase. BSE images confirm this, shown in Fig. 1(c), in the clearer inter-dendritic regions. The average chemical composition of the $FeCoNiCu_{1.15}$ solid solution features up to 21 at. % Cu together with Fe (24 at. %), Co (28 at. %) and Ni (27 at. %). The remaining copper precipitates in the Cu-rich phase, together with a small amount of Ni, Fe, and Co.

When V and Cu are both combined with Fe, Co and Ni, the solidification process changes once again, see Fig. 1(d). A solid solution is formed that contains V–Fe–Co–Ni–Cu. However, its chemical composition differs from the nominal composition due to the lack of solubility between V and Cu, which induces a decrease in Cu-content from 21 at. % in $FeCoNiCu_{1.15}$ to 13 at. %. The ratio of the remaining ferromagnetic elements is Fe (22 at. %), Co (24 at. %) and Ni (23 at. %), while V remains close to 17 at. %. The remaining Cu is seen as spheres and rounded elements in a Cu-rich phase in Fig. 1(d). This could be an indication of liquid phase immiscibility between a Cu-rich liquid and V–Fe–Co–Ni–Cu solid solution, as Fe, Co and especially V tend to phase-separate with Cu (see also Fig. 2). A similar morphology is observed in $Nb_xFeCoNiCu$ [33]. This secondary liquid formation is also observed in the CALPHAD plot in Fig. 2(d), as it predicts the segregation of a secondary Cu-rich liquid from a main liquid at around 1500 K.

In addition to the two ccp phases, an amount of removed sample is seen, related to the formation of the sigma phase. The sigma phase appears around a ccp phase containing V–Fe–Co–Ni–Cu (main SS) and the Cu-rich phase. The sigma phase fraction estimated from image analysis is 1.1% in volume. This time, it exhibits a different morphology than the one seen for the 4-element $V_{0.85}$FeCoNi alloy. It is precipitated in spheres or dendrites (snowflakes), see Fig. 1(d). This can be related to a different interfacial energy between the liquid and the solid formation of the V-containing intermetallic. A three-phase system is thus present, with a Cu-rich SS, a sigma intermetallic and a main V–Fe–Co–Ni–Cu solid solution.

The different elements present in each of the solid solutions allows for studying 4 different magnetic systems: (i) purely ferromagnetic interactions in the 3-element alloy (FeCoNi), (ii) ferromagnetic elements (FeCoNi) alloyed with a diamagnetic element (Cu) which dilutes the moments, (iii) ferromagnetic elements (FeCoNi) alloyed with an element that induces antiparallel interactions (V), and finally, (iv) the combination of dilution and antiparallel coupling in the 5-element ferromagnetic alloy (V–Fe–Co–Ni–Cu).

With the main compositions identified, it is necessary to determine the lattice parameters of the phases present. The PXD patterns of the four solid solutions are shown in Fig. 3 and are primarily attributed to ccp structures with no other observed reflections. The lattice parameters are presented in Table 2 In the as-cast state, FeCoNi has an *a*-axis of 3.571(2) Å. By addition of V and Cu, *a* is slightly altered to3.595(2) Å for both. Upon simultaneous addition of V and Cu, the *a*-axis increases slightly to 3.604(2) Å. The stacking faults probability in the ccp lattice is obtained from the FAULTS software refinement, and shown in Table 2. Stacking faults in HEAs are common due to the high number of elements, as they tend to lower the stacking fault energy [34,35]. The stacking fault probabilities ranged from 8 to 14% between the alloys and the change in values may be ascribed to the presence of different elements and the level of strain in the powder for the PXD sample preparation.

### 3.2. Magnetic properties of the main solid solutions

Fig. 4 depicts magnetization as a function of temperature for the four alloys in the vicinity of $T_C$ with applied fields of 1 T. Data was obtained with a VSM in the range from 300 to 1100 K and by PPMS from 10 to 370 K. To facilitate comparison to the DFT results, magnetization values are expressed in Bohr magnetons in the left axis, and in $Am^2/kg$ on the right axis. High magnetic fields were selected to better correlate to the intended application, where fields of at least 1 T will be employed to generate the magnetocaloric effect. By normalizing the temperature by $T_C$, one can compare materials with different $T_C$ and gain insight on the thermal dependence of the magnetic moments in the solid solution. The $\Delta S_m$ of $V_{0.85}FeCoNiCu_{1.15}$ alloys was investigated in a previous report [14] and therefore $\Delta S_m$ calculations are not performed in this study. Instead, the absolute derivative of magnetization as a function of temperature is depicted in Fig. 4(b) with an applied magnetic field of $\mu_0 H = 1$ T. While it does not replace the $\Delta S_m$ curves, high $|dM/dT|$ values are an indication of a high $\Delta S_m$. The high field $|dM/dT|$ can provide insight

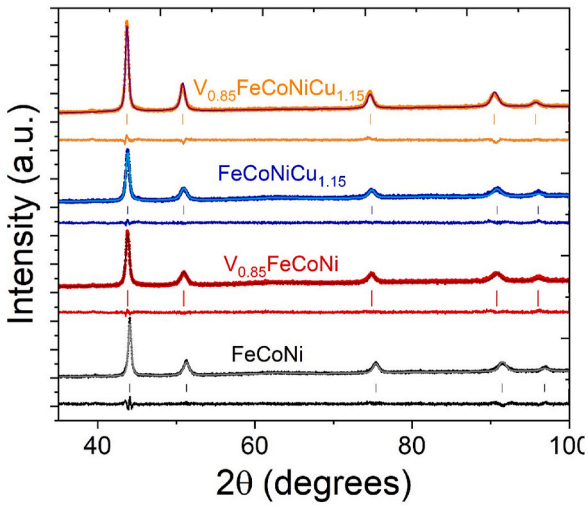


**Fig. 3.** (Color online.) PXD patterns and Rietveld refinements of the four studied alloys measured with Cu-Kα radiation (λ = 1.5409 Å). Observed intensities are shown as points, calculated intensities as lines and difference plots are shown below each pattern.

**Table 2**
Experimental lattice parameters (*a*), *Curie* temperatures ($T_C$), and saturation magnetizations ($M_S$) of the studied FeCoNi-based alloys.

| main phase composition (formula units) | Exp. *a*. (Å) | Stacking fault probability (%) | $\chi^2$ | exp. $T_C$ (K) | Exp. $M_S$ ($\mu_B$/atom) |
|---|---|---|---|---|---|
| $Fe_1Co_{1.14}Ni_{1.14}$ | 3.571 (2) | 8.4% | 1.39 | 997 | 1.47 |
| $FeCo_{1.16}Ni_{1.09}Cu_{0.84}$ | 3.595 (2) | 14.2% | 1.38 | 957 | 1.16 |
| $V_{0.82}FeCo_{1.07}Ni_{1.03}$ | 3.595 (2) | 13.6% | 1.26 | 245 | 0.58 |
| $V_{0.75}FeCo_{1.07}Ni_{1.01}Cu_{0.56}$ | 3.604 (2) | 8.4% | 1.7 | 278 | 0.54. |

on the shape of $\Delta S_m$ curves, and approximate values if the $|dM/dT|$ values are multiplied by the applied field in T, without the arduous process of obtaining a series of isofield or isotherm curves for a $\Delta S_m$ calculation.

In the FeCoNi base alloy, a ferromagnetic-to-paramagnetic transition is observed. The ferromagnetic state is stabilized due to the large external magnetic field, leading to a broad curve that spans tens of K. The maximum change of magnetization is observed at 997 K, as shown in Table 2 together with all experimentally observed $T_C$'s. The total saturation magnetization ($M_S$) for this alloy is 1.47 $\mu_B$/atom. With the introduction of Cu, $M_S$ is decreased to 1.16 $\mu_B$/atom, and the derivative (dM/dT) is slightly smaller; however, the overall behaviour characteristic of a ferromagnetic material is kept. This is also evident from Fig. 4 (b) which shows the derivative of magnetization as a function of temperature, (dM/dT) as $FeCoNiCu_{1.15}$ ($T_C$ = 957 K) exhibits a similar behaviour as FeCoNi. This leads to the conclusion that other elements besides Cu such as Cr, V and Mn are necessary to lower $T_C$, confirming the work by Kurniawan et al. [7].

In samples containing V, where antiparallel interactions are inserted into the magnetic system, the temperature dependence of magnetization changes drastically and the magnetic transition becomes much broader than for FeCoNi and $FeCoNiCu_{1.15}$. Furthermore, $M_S$ is largely decreased to 0.58 and 0.54 $\mu_B$/atom in $V_{0.85}FeCoNi$ and $V_{0.85}FeCoNiCu_{1.15}$, respectively.

The magnetic transitions for $V_{0.85}FeCoNi$ and $V_{0.85}FeCoNiCu_{1.15}$ are presented in Fig. 5, in the temperature range from 10 to 375 K. A measurement artifact is observed as a slight increase in magnetization at T = 50 K for both samples. In the case of $V_{0.85}FeCoNi$, the measured $T_C$ is 245 K, while $V_{0.85}FeCoNiCu_{1.15}$ presents a $T_C$ of approx. 280 K. The absolute magnetization values are higher for the sample without Cu, as it acts as a dilutant for the ferromagnetic moments. On both V-containing alloys there is still some remaining magnetization after the end of the measurement range due to the large number of exchange interactions and inhomogeneity in the alloy. Surprisingly, the (dM/dT) derivative of the 5-element alloy is higher. This can be explained by the smaller V-content in the 5-element solid solution (18 at. %) compared to the 4-element alloy (21 at. %). The decrease in (dM/dT) seen in Fig. 4(b) due to the introduction of V is a hindrance to the magnetocaloric properties. This can be correlated to local inhomogeneities between V and the other elements, creating a distribution of $T_C$'s. The slightly larger derivative seen in Fig. 5 for $V_{0.85}FeCoNiCu_{1.15}$ compared to $V_{0.85}FeCoNi$ could hint at a pathway for improving the magnetocaloric

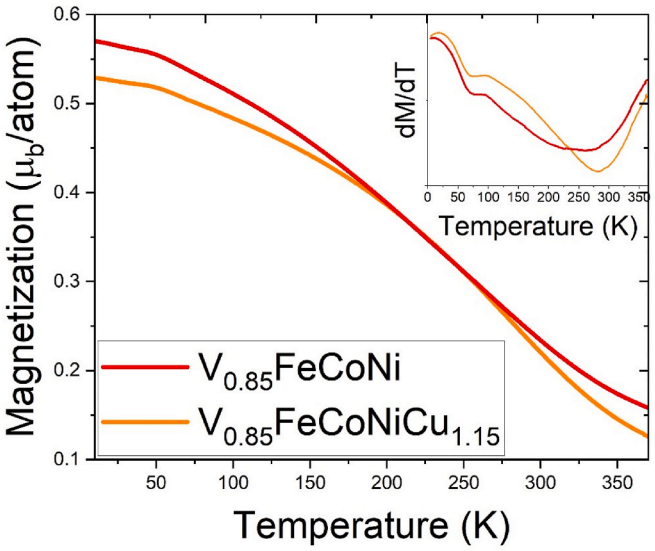


**Fig. 5.** (Color online.) Magnetization as a function of temperature for two V-containing alloys, with applied field of $\mu_0H$ = 1 T. The inset shows the derivative of magnetization (dM/dT) as a function of temperature. A measurement artifact occurring due to impurities in the sample chamber is seen at T = 50 K.

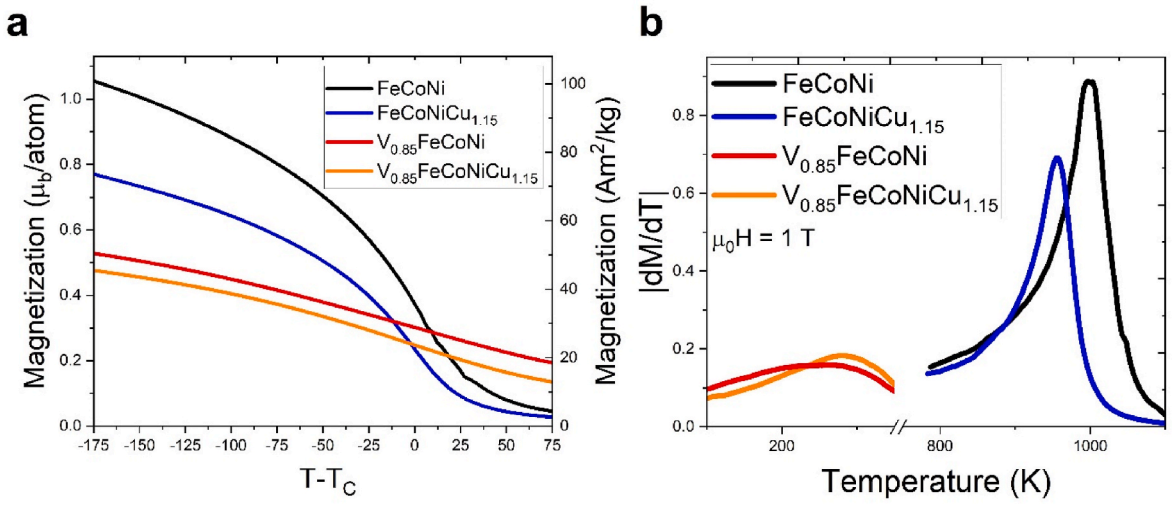


**Fig. 4.** (Color online.) (a) Magnetization as a function of temperature for the four studied alloys with applied fields of $\mu_0H$ = 1 T, in Bohr magneton/atom on the left, and in $Am^2$/kg on the right. (b) Absolute derivative of magnetization as a function of temperature for the studied alloys, allowing one to compare the transitions with each modification. With the introduction of Cu, a decrease in absolute magnetization is observed, but the overall behaviour is unchanged. In V-containing alloys, absolute magnetization, and derivatives of magnetization (dM/dT) are strongly modified, which is harmful to the magnetocaloric effect.

properties by modifying the ratio between dilution and antiferromagnetic elements and the ferromagnetic elements. This is exactly the case observed by Belyea et al. in $CrFeCoNiPd_x$. With larger contents of Pd, the nominal content of Cr decreases from 25 at. % (x = 0) to 22.2 at. % (x = 0.5). This modifies $T_C$'s from around 100 K to300 K [5].

### 3.3. Theoretical results

Electronic structure calculations and Monte Carlo simulations are presented in detail for the nominal composition of the 3-, 4- and 5-element alloys, where the Fe, Co and Ni content is equal. The nominal atomic concentrations of the elements are listed in the upper section of Table 1. For these alloys, the 0 K equilibrium lattice parameters, *a*, were estimated from a Morse type of equation of state as described in Section 2.1. Due to the quick solidification of the as-cast samples, we expect a solid solution with the greatest extent of randomness of the constituting elements, and we can furthermore assume that the composition of the FeCoNi sample in the as-cast state is very close to the nominal composition. Within this set of assumptions, we find that the lattice parameter of FeCoNi (3.56 Å) is in good agreement with the measured data (3.57 Å) while its total magnetic moment ($m_{tot}$) per 1 atom calculated at 0 K is 1.64 $\mu_B$. This compares well to the measured value of 1.47 $\mu_B$ at RT. These results give us confidence in the theoretical framework and allow us to investigate how the addition of Cu and V affect the magnetic properties of FeCoNi-based alloys.

Fig. 6 presents the element resolved partial densities of states (DOS) for Fe, Co, and Ni in the equiatomic FeCoNi base alloy. The difference in DOS modifies the individual magnetic moments for each of the elements, depicted in Table 3. The largest exchange splitting between the spin-up and spin-down DOS is manifested for Fe. The spin-up channel is almost filled, and the remaining number of electrons occupy the spin-down channel resulting in a magnetic moment of 2.51 $\mu_B$ for Fe. Co and Ni possess more electrons than Fe, that will result in a complete filling of the spin-up states showing larger values of DOS in the energy range of −0.25 to −0.05 Ry for Co and Ni than for Fe. Also, the peak at −0.05 Ry is slightly shifted towards lower energies for Co and Ni compared to Fe. The extra electrons for Co and Ni are accommodated by the spin-down channel resulting in decreased local magnetic moments of 1.69 $\mu_B$ (Co) and 0.72 $\mu_B$ (Ni), respectively, compared to Fe.

To compare the effect of adding Cu and V to FeCoNi, we turn our attention to $FeCoNiCu_{1.15}$ and $V_{1.15}FeCoNi$, where the nominal atomic concentration and the ratio of Fe, Co and Ni are identical. The modelled lattice parameters of $FeCoNiCu_{1.15}$ and $V_{1.15}FeCoNi$ are both slightly larger than for FeCoNi. The V-containing 4 element alloy has a lattice parameter of 3.59 Å due to the larger volume of the element V. In the case of $FeCoNiCu_{1.15}$, the calculated lattice parameter of 3.59 Å can be ascribed to filled *d*-orbitals of Cu, imposing larger bond lengths. In the 5-element alloy, the combined effect of V and Cu increases the calculated lattice parameter slightly to 3.60 Å.

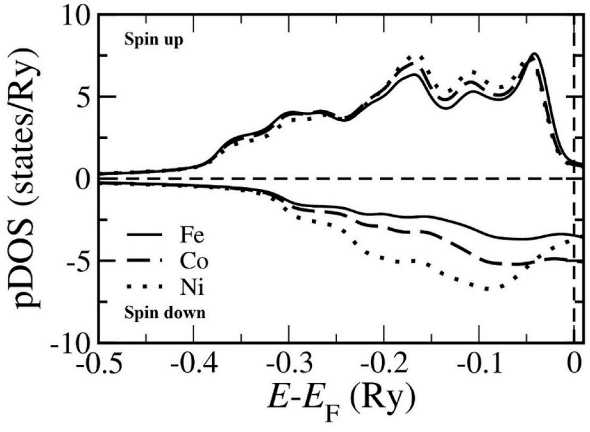


**Fig. 6.** Partial density of states (pDOS) for Fe (full line), Co (dashed line), and Ni (dots) in the FeCoNi equiatomic base alloy.

The element-resolved and total magnetic moments for different FeCoNi-based multicomponent alloys are listed in Table 3. The addition of electrons to FeCoNi, *e.g.,* via Cu in $FeCoNiCu_{1.15}$, affects the local magnetic moments of Fe, Co, and Ni differently. The extra electrons from Cu fill completely the spin-up states for Fe, see the upper panel of Fig. 7, inducing a subtle increase of $m_{Fe}$. The filled spin-up channel of Co and Ni cannot accommodate more electrons; here the spin-down states receive the extra electrons (see middle and lower panels of Fig. 7 for Co and Ni, respectively) resulting in a decrease of $m_{Co}$ and $m_{Ni}$. The addition of V in $V_{1.15}FeCoNi$ has the opposite effect: electrons are removed from both spin-up and spin-down channels of the pDOS of Fe, Co, and Ni, resulting in a drastic decrease of $m_{Fe}$, $m_{Co}$ and $m_{Ni}$. The induced moment on Cu is very small for all compounds (< 0.05 $\mu_B$). On the other hand, the local moment induced on V is quite substantial and comparable to $m_{Ni}$ (see Table 3), and it couples antiparallel to the moments of the magnetic elements (Fe, Co, Ni), thereby reducing the ferromagnetic character of the alloy.

These changes in the electronic structure and magnetic moments translate to the exchange integrals calculated for the 3- and 4-component alloys plotted in Figs. 8 and 9. All magnetic pair interactions are positive in case of FeCoNi establishing a ferromagnetic ground state. $J_{Fe\text{-}Co}$ and $J_{Co\text{-}Co}$ have the largest values while $J_{Fe\text{-}Ni}$ and $J_{Co\text{-}Ni}$ are half of them. Adding Cu to FeCoNi results in a very small increase of the 1st nearest neighbor (NN) $J_{Fe\text{-}Fe}$, $J_{Fe\text{-}Co}$ and $J_{Co\text{-}Co}$ while their 2nd NN pair interactions are decreased. $J_{Fe\text{-}Ni}$ and $J_{Co\text{-}Ni}$ are not affected by the addition of Cu. Since the nominal concentration of Fe, Co and Ni decreases considerably in $FeCoNiCu_{1.15}$ (24.1 at. %) compared to the equiatomic alloy (33 at. %), and Cu does not contribute to the magnetic properties (due to its very small induced magnetic moment), we expect a lower $T_C$ for $FeCoNiCu_{1.15}$ than for FeCoNi.

In contrast, adding V largely affects the magnetic exchange interactions in two ways. Firstly, we observe a significant decrease in all pair interactions between Fe, Co, and Ni for $V_{1.15}FeCoNi$. Secondly, V couples antiferromagnetically to Fe and Co. Due to this drastic change we can anticipate a large decrease of $T_C$ for $V_{1.15}FeCoNi$ compared to both FeCoNi and $FeCoNiCu_{1.15}$. Decreasing the amount of V in $V_{0.85}FeCoNi$ leads to an increase of $J_{ij}$'s, anticipating a larger $T_C$ than for $V_{1.15}FeCoNi$.

The combination of V and Cu in the 5-element alloy $V_{0.85}FeCoNiCu_{1.15}$ will result in intermediate values for $J_{Fe\text{-}Fe}$, $J_{Fe\text{-}Co}$ and $J_{Co\text{-}Co}$ compared to the 3- and 4-element alloys FeCoNi, $FeCoNiCu_{1.15}$ and $V_{0.85}FeCoNi$, respectively. Compared to $V_{0.85}FeCoNi$, the dilution with Cu in the 5-element alloy has no large effect on $J_{Fe\text{-}Ni}$ and $J_{Co\text{-}Ni}$. However, they are still low (0.25 mRy) when compared to $J_{Fe\text{-}Ni}$ and $J_{Co\text{-}Ni}$ in FeCoNi and $FeCoNiCu_{1.15}$ (See the top-left part of Fig. 9). In the 5-element alloy, $J_{Fe\text{-}V}$ and $J_{Co\text{-}V}$ have the largest negative values (antiparallel couplings).

The Curie temperatures calculated by the Monte Carlo method from ferromagnetic exchange interactions for the 3-, 4- and 5-element alloys assuming nominal compositions are listed in Table 3. The magnetic transition temperature for FeCoNi is calculated to 1009 K based on the theoretical lattice parameter. Cu-addition increases the 1st NN $J_{i-j}$ 's slightly compared to that of FeCoNi. However, $T_C$ of $FeCoNiCu_{1.15}$ (820 K) is lower than for the FeCoNi alloy. This is the result of a dilution effect caused by Cu since the concentration of the magnetic elements are lower in $FeCoNiCu_{1.15}$ than in FeCoNi (see Table 1). In addition, Cu does not contribute to the magnetism, due to its filled *d*-orbitals that manifest in a negligible induced magnetic moment. As expected from the analysis of the exchange interactions, the lowest Curie temperature (233 K) is obtained for $V_{1.15}FeCoNi$ while increasing Fe, Co, and Ni concentrations in $V_{0.85}FeCoNi$, compared to $V_{1.15}FeCoNi$ (see Table 1) increases $T_C$ to 350 K (see Table 3). The addition of Cu to the V-alloy decreases not only the atomic concentration of V, but also the concentration of the magnetic

**Table 3**
Element resolved magnetic moments, $m_i$ ($\mu_B$/atom), total magnetic moment, $m_{tot}$ ($\mu_B$/atom), and calculated $T_C$ (K) for the nominal and measured compositions of the solid solutions. Nominal compositions are written in italic.

| System | Composition | $m_{Fe}$ ($\mu_B$/atom) | $m_{Co}$ ($\mu_B$/atom) | $m_{Ni}$ ($\mu_B$/atom) | $m_V$ ($\mu_B$/atom) | $m_{tot}$ ($\mu_B$/atom) | Calc. $T_C$ (K) | Experimental $T_C$ (K) |
|---|---|---|---|---|---|---|---|---|
| Fe–Co–Ni | *FeCoNi* | *2.51* | *1.69* | *0.72* | | *1.64* | *1009* | |
| | $FeCo_{1.14}Ni_{1.14}$ | 2.65 | 1.67 | 0.64 | – | 1.61 | 997 | 1018 |
| Fe–Co–Ni–Cu | *$FeCoNiCu_{1.15}$* | *2.56* | *1.65* | *0.61* | - | *1.19* | *820* | |
| | $FeCo_{1.16}Ni_{1.09}Cu_{0.84}$ | 2.70 | 1.66 | 0.58 | – | 1.29 | 871 | 957 |
| V–Fe–Co–Ni | *$V_{1.15}FeCoNi$* | *1.93* | *1.00* | *0.23* | *−0.44* | *0.64* | *233* | |
| | *$V_{0.85}FeCoNi$* | *2.05* | *1.16* | *0.31* | *−0.56* | *0.79* | *350* | |
| | $V_{0.82}FeCo_{1.07}Ni_{1.03}$ | 2.22 | 1.22 | 0.31 | −0.74 | 0.83 | 384 | 245 |
| V–Fe–Co–Ni–Cu | *$V_{0.85}FeCoNiCu_{1.15}$* | *2.21* | *1.23* | *0.29* | *−0.54* | *0.66* | *362* | |
| | $V_{0.75}FeCo_{1.07}Ni_{1.01}Cu_{0.56}$ | 2.32 | 1.27 | 0.31 | −0.75 | 0.76 | 403 | 278 |

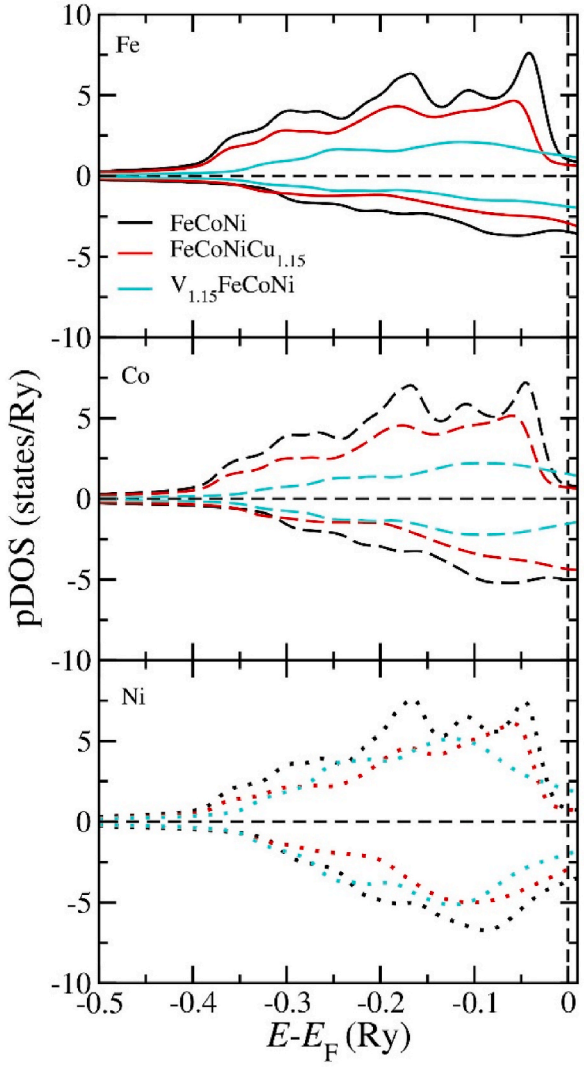


**Fig. 7.** (Color online.) pDOS for Fe, Co, and Ni in various multicomponent alloys. Black line stands for FeCoNi, the red line for $FeCoNiCu_{1.15}$ and the blue line for $V_{1.15}FeCoNi$. Full line stands for Fe, the dashed line for Co and the dotted line for Ni.

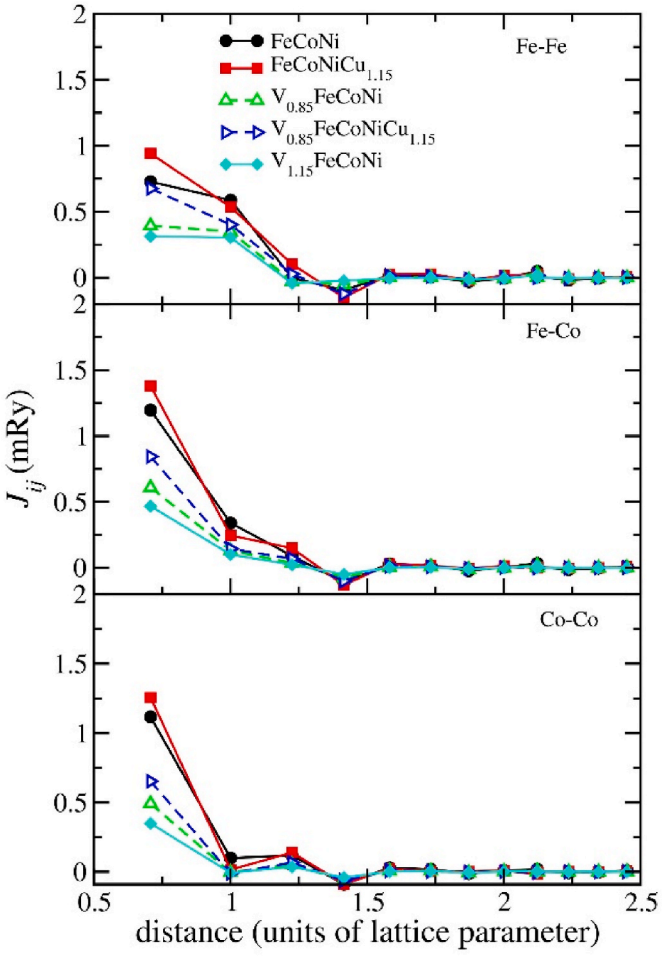


**Fig. 8.** (Color online.) Calculated magnetic pair exchange interactions for (Fe–Fe), (Fe–Co), and (Co–Co) in the FeCoNi base alloy and selected V- and Cu-doped based solid solutions.

elements (see Table 1). Therefore, the $T_C$ of $V_{0.85}FeCoNiCu_{1.15}$ (362 K) is higher compared to the V-alloys.

From the above analysis based on the nominal compositions, we can conclude that Cu moderately dilutes the ferromagnetic interactions between Fe, Co and Ni and shields the negative coupling of V, resulting in moderate changes in $T_C$ of $FeCoNiCu_{1.15}$ compared to FeCoNi, and of $V_{0.85}FeCoNiCu_{1.15}$ compared to $V_{1.15/0.85}FeCoNi$. On the other hand, V acts in three different ways: it dilutes the concentration of the magnetic elements, decreases their pair magnetic interactions and couples antiparallel to them. This leads to a drastic decrease of $T_C$ for the V-containing alloys.

The effect of other 3d metals such as Ti, Cr and Mn on the magnetism of the FeCoNi-base alloy is now briefly discussed. In $X_{1.15}FeCoNi$, where X = Ti, Cr and Mn, the randomly distributed X-elements have a similar effect on the local magnetic moments of Fe, Co, and Ni as V; namely, $m_{Fe}$, $m_{Co}$ and $m_{Ni}$ decrease. In addition, a quite substantial induced local moment develops on Ti (−0.34 $\mu_B$), comparable with the Ni moment

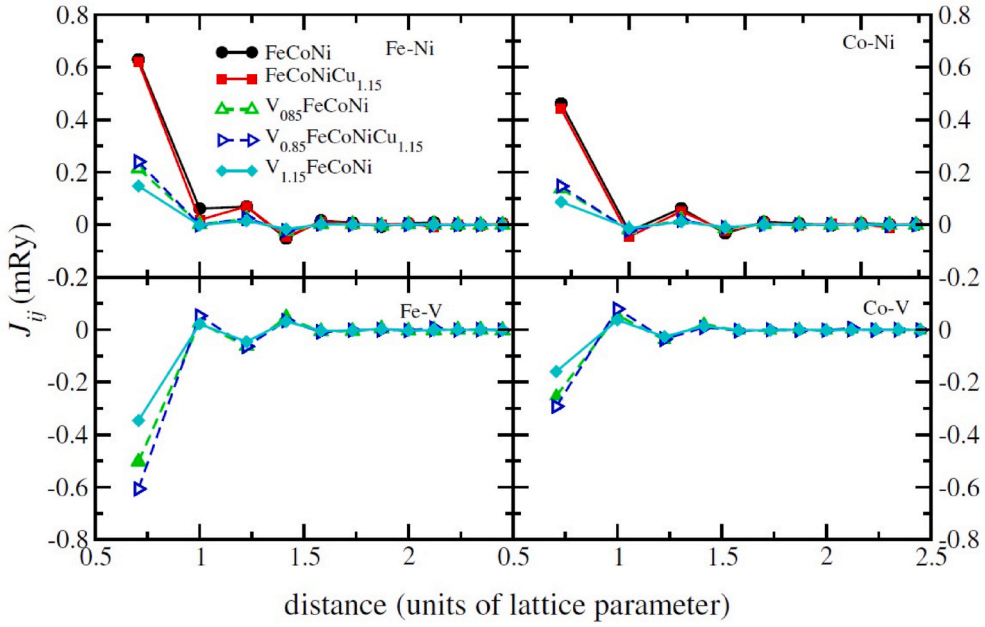


**Fig. 9.** (Color online.) Calculated magnetic pair exchange interactions for (Fe–Ni), (Co–Ni), (Fe–V) and (Co–V) in the FeCoNi base alloy and selected V- and Cu-doped based solid solutions.

(0.24 $\mu_B$), that couples antiparallel to the local moment of the ferromagnetic elements. $m_{Cr}$ and $m_{Mn}$ are also quite high, with $-0.62$ $\mu_B$ (Cr) and $-1.72$ $\mu_B$ (Mn), respectively, and couple antiparallel to the moments of Fe, Co, and Ni, as expected. Therefore, we expect that the effect of Ti, Cr, and Mn on the high temperature magnetism of $X_{1.15}FeCoNi$ is like that of V. Consequently, we foresee a large decrease of $T_C$ for these compounds. Indeed, the decrease of $T_C$ for $X_{1.15}FeCoNi$ (X = Ti, Cr and Mn, respectively), estimated via mean field approximation is large as in the case of V. However, a detailed investigation on the effect of Ti, Cr and Mn is beyond the scope of the present study.

Magnetic properties have also been calculated for the experimentally measured compositions and lattice parameters and are also listed in Table 3. The total magnetic moment calculated for $FeCo_{1.14}Ni_{1.14}$ at 0 K is about 10% larger than at RT. This discrepancy is even larger for the alloys that contain V and Cu. The experimental trends are however captured by the theory. The calculated $T_C$s for $FeCo_{1.14}Ni_{1.14}$ and $FeCo_{1.16}Ni_{1.09}Cu_{0.84}$ based on the experimental lattice parameters, are 996 K and 871 K, respectively. They are in good agreement with the measured data, 997 K and 957 K, respectively. In contrast, we find a large discrepancy for the V-containing alloys. This is not surprising considering the applied unavoidable assumptions and approximations. Firstly, $J_{i-j}$'s are calculated for the ideal atomic positions, *e.g.,* unrelaxed lattice positions neglecting the local lattice relaxations due to the size differences between the elements. The second assumption is the random distribution of the elements that does not consider the effect of short-range order or segregation that are possibly present in real alloys. Finally, the temperature effect on the magnitude of the local magnetic moments and as a consequence on the exchange parameters (non-Heisenberg behaviour), that is widely discussed recently [36–41], is also not investigated in this study.

Although the actual values of the total magnetic moment and $T_C$ for the as-cast alloys with V addition do not agree with the measured data, these properties are a direct consequence of the average interactions across the material. In the calculations, the modelled system is still an idealized solid solution. On the other hand, a closer look on the enthalpies of mixing of the studied alloys can shed some light on the trends observed in the experiments. As is known from literature, an enthalpy of mixing, $\Delta H_{mix}$, very close to 0 in connection with atomic size differences $\leq 6.6\%$ favours the formation of solid solutions [42]. This is the case for the nominal composition of $V_{0.85}FeCoNiCu_{1.15}$, with a $\Delta H_{mix}$ of 0.32 J/K. However, this value is only accidently close to 0 because it results from a combination of pairs with large negative $\Delta H_{mix}$ (Co–V and Ni–V), and others with a large positive $\Delta H_{mix}$ (Fe–Cu, Co–Cu and Cu–V) that can individually promote segregation. Nevertheless, we are confident that the conclusions drawn for the nominal compositions are also valid for the as-cast samples.

## 4. Conclusion

Four ferromagnetic transition-metal based alloys were studied to understand how structure and microstructure affect the steepness of the magnetic transition, which is an indication of the magnetocaloric effects in the materials. All alloys were studied in metastable states after casting. Pure ferromagnetic, diluted ferromagnetic, ferromagnetic-antiferromagnetic and diluted ferromagnetic-antiferromagnetic systems were investigated.

The FeCoNi base alloy exhibits a monophasic microstructure. With the addition of V, a sigma intermetallic is introduced, while with Cu, a secondary Cu-rich phase is precipitated in an inter-dendritic region due to the lack of solubility at lower temperatures. In the 5-element alloy $V_{0.85}FeCoNiCu_{1.15}$, a sigma intermetallic and secondary ccp phase are both present. However, instead of precipitating from a main solid solution, the Cu-rich phase is solidified from a secondary liquid phase, as indicated from the morphology of the Cu-rich phase.

The precipitation of secondary phases impacts the chemical composition of the main solid solutions, which is directly responsible for the macroscopic magnetization behaviour. All studied solid solutions feature ferromagnetism at lower temperatures and undergo ferro-to-paramagnetic transitions. The temperature dependent magnetization curves show that FeCoNi has a typical second order transition, with a continuous decrease in magnetization. The dilution induced by the addition of Cu in $FeCoNiCu_{1.15}$ mostly impacts the magnetization values, and slightly effects $T_C$ values and the steepness of the magnetic transition. The introduction of V, however, in V–FeCoNi strongly modifies $T_C$, decreasing it below room temperature in $V_{0.85}FeCoNi$. The absolute magnetization values are reduced, and the transition is broadened, which are both detrimental for magnetocaloric properties. The 5-element alloy $V_{0.85}FeCoNiCu_{1.15}$ boasts a similar magnetic behaviour,

though with a slightly increased derivative of magnetization that is credited to the reduced V content.

Analysis of the magnetic properties by DFT shows that the addition of Cu to FeCoNi dilutes the magnetic exchange and results in a slight decrease of $T_C$. In contrast, the addition of V acts in three different ways: (i) V dilutes the amount of the ferromagnetic elements; (ii) its induced moment couples antiparallel to the moments of Fe, Co, and Ni; (iii) the addition of V leads to a decrease of the magnetic exchange interactions between the ferromagnetic elements. These combined effects result in a large decrease of the magnetic transition temperature in the studied $V_{0.85}FeCoNi$ and $V_{0.85}Fe_1Co_1Ni_1Cu_{1.15}$ alloys. A similar behaviour is predicted for other early 3 *d*-transition metals based on a brief investigation of their effect on the local magnetic moments of $X_{1.15}FeCoNi$ (X = Ti, Cr and Mn), though in different strengths.

To make high entropy alloys viable for magnetocaloric applications, the strength of ferromagnetic interactions is of key importance, together with the abruptness of the transition (high dM/dT). The drastic reduction of $T_C$ that is caused by the addition of V, Mn, Cr and Ti to the FeCoNi base alloy is remarkable. However, such elements are also responsible for a large decrease in the moments of Fe, Co, and Ni. Pathways to improvement of the magnetocaloric effect lie in optimizing the content of antiferromagnetic coupling and diluting elements.

## Credit roles

**Bruno G. F. Eggert:** Conceptualization (equal)Data curation (equal) Formal analysis (equal) Investigation (equal) Methodology (equal) Visualization (equal) Writing - original draft (equal) Writing - review & editing (equal) **Erna K. Delczeg-Czirjak:** Software (equal)Methodology (equal) Formal analysis (equal) Resources (equal) Visualization (equal) Writing – original draft (equal) Writing - review & editing (equal) **Bjørn Hauback:** Supervision (equal)Writing - review & editing (equal) **Christoph Frommen:** Funding acquisition (equal)Project administration (equal) Supervision (equal) Writing - review & editing (equal).

## Declaration of competing interest

The authors declare that they have no known competing financial interests or personal relationships that could have appeared to influence the work reported in this paper.

## Data availability

Data will be made available on request.

## Acknowledgements

This work was financed by The Research Council of Norway through the NANO2021 program, Project No. 287150. E. K. D.-Cz. acknowledges the Swedish National Infrastructure for Computing (SNIC) for computational resources (snic2021-1-36 and snic2021-5-340) and the Swedish Foundation for Strategic Research (SSF) (contract EM-16-0039) for financial support. Valuable discussions with A.V. Ruban from KTH Royal Institute of Technology and M. Pereiro from Uppsala University are also acknowledged. B. G. F. Eggert also acknowledges Björn M. Valldor for his skillful assistance on performing magnetic measurements at low temperatures.

## References

[1] A. Kitanovski, Energy Applications of Magnetocaloric Materials, 2020: 1903741, https://doi.org/10.1002/aenm.201903741.
[2] V. Franco, J.S. Blázquez, J.J. Ipus, J.Y. Law, L.M. Moreno-Ramírez, A. Conde, Magnetocaloric effect: from materials research to refrigeration devices, Prog. Mater. Sci. 93 (2018) 112–232, https://doi.org/10.1016/j.pmatsci.2017.10.005.
[3] M.C. Gao, D.B. Miracle, D. Maurice, X. Yan, Y. Zhang, J.A. Hawk, High-entropy functional materials, J. Mater. Res. 33 (2018) 3138–3155, https://doi.org/10.1557/jmr.2018.323.
[4] S.M. Na, P.K. Lambert, H. Kim, J. Paglione, N.J. Jones, Thermomagnetic properties and magnetocaloric effect of FeCoNiCrAl-type high-entropy alloys, AIP Adv. 9 (2019), https://doi.org/10.1063/1.5079394.
[5] D.D. Belyea, M.S. Lucas, E. Michel, J. Horwath, C.W. Miller, Tunable magnetocaloric effect in transition metal alloys, Sci. Rep. 5 (2015) 1–8, https://doi.org/10.1038/srep15755.
[6] A. Perrin, M. Sorescu, M.T. Burton, D.E. Laughlin, M. McHenry, The role of compositional tuning of the distributed exchange on magnetocaloric properties of high-entropy alloys, Jom 69 (2017) 2125–2129, https://doi.org/10.1007/s11837-017-2523-3.
[7] M. Kurniawan, A. Perrin, P. Xu, V. Keylin, M. McHenry, Curie temperature engineering in high entropy alloys for magnetocaloric applications, IEEE Magn. Lett. 7 (2016) 1–5, https://doi.org/10.1109/LMAG.2016.2592462.
[8] N.A. Morley, B. Lim, J. Xi, A. Quintana-Nedelcos, Z. Leong, Magnetic properties of the complex concentrated alloy system CoFeNi0.5Cr0.5Alx, Sci. Rep. 10 (2020) 1–12, https://doi.org/10.1038/s41598-020-71463-3.
[9] D.B. Miracle, O.N. Senkov, A critical review of high entropy alloys and related concepts, Acta Mater. 122 (2017) 448–511, https://doi.org/10.1016/j.actamat.2016.08.081.
[10] Z. Dong, S. Huang, V. Ström, G. Chai, L.K. Varga, O. Eriksson, L. Vitos, MnxCr0.3Fe0.5Co0.2Ni0.5Al0.3 high entropy alloys for magnetocaloric refrigeration near room temperature, J. Mater. Sci. Technol. 79 (2021) 15–20, https://doi.org/10.1016/j.jmst.2020.10.071.
[11] A. Phys, Magnetocaloric Properties of Melt-Spun MnFe-Rich High-Entropy Alloy Magnetocaloric Properties of Melt-Spun MnFe-Rich High-Entropy Alloy, 2021: 141909, https://doi.org/10.1063/5.0065067.
[12] M.S. Lucas, D. Belyea, C. Bauer, N. Bryant, E. Michel, Z. Turgut, S.O. Leontsev, J. Horwath, S.L. Semiatin, M.E. McHenry, C.W. Miller, Thermomagnetic analysis of FeCoCrxNi alloys: magnetic entropy of high-entropy alloys, J. Appl. Phys. 113 (2013) 2011–2014, https://doi.org/10.1063/1.4798340.
[13] A. Quintana-Nedelcos, Z. Leong, N.A. Morley, Study of dual-phase functionalisation of NiCoFeCr-Alx multicomponent alloys for the enhancement of magnetic properties and magneto-caloric effect, Mater. Today Energy 20 (2021): 100621, https://doi.org/10.1016/j.mtener.2020.100621.
[14] B.G.F. Eggert, E.K. Delczeg-czirjak, F. Maccari, S. Kumar, O. Gutfleisch, H. Fjellvåg, B.C. Hauback, C. Frommen, Exploring V-Fe-Co-Ni-Al and V-Fe-Co-Ni-Cu high entropy alloys for magnetocaloric applications, J. Alloys Compd. 921 (2022): 166040, https://doi.org/10.1016/j.jallcom.2022.166040.
[15] T. Gottschall, K.P. Skokov, M. Fries, A. Taubel, I. Radulov, F. Scheibel, D. Benke, S. Riegg, O. Gutfleisch, Making a cool choice: the materials library of magnetic refrigeration, Adv. Energy Mater. 9 (2019), https://doi.org/10.1002/aenm.201901322.
[16] J.P. Perdew, K. Burke, M. Ernzerhof, Generalized gradient approximation made simple, Phys. Rev. Lett. 77 (1996) 3865–3868, https://doi.org/10.1103/PhysRevLett.77.3865.
[17] J. Rodriguez-Carvajal, Recent developments of the program FULLPROF, commission on powder diffraction, IUCr Newsl. (Int. Union Crystallogr.) 26 (2001) 12–19. http://www.iucr.org/iucr-top/comm/cpd/html/newsletter26.html.
[18] C.A. Schneider, W.S. Rasband, K.W. Eliceiri, NIH Image to ImageJ: 25 years of image analysis, Nat. Methods 9 (2012) 671–675, https://doi.org/10.1016/S0031-8914(53)80099-6.
[19] O.K. Andersen, O. Jepsen, G. Krier, Lectures on Methods of Electronic Structure Calculation, 1994.
[20] L. Vitos, The EMTO Method and Applications in Computational Quantum Mechanics for Materials Engineers, Springer-Verlag London, 2007.
[21] P. Soven, Coherent-potential model of substitutional disordered alloys, Phys. Rev. 156 (1967) 809–813, https://doi.org/10.1103/PhysRev.156.809.
[22] B.L. Gyorffy, Coherent-potential approximation for a nonoverlapping-muffin-tin-potential model of random substitutional alloys, Phys. Rev. B 5 (1972) 2382–2384, https://doi.org/10.1103/PhysRevB.5.2382.
[23] L. Vitos, Total-energy method based on the exact muffin-tin orbitals theory, Phys. Rev. B 64 (2001): 14107, https://doi.org/10.1103/PhysRevB.64.014107.
[24] A. V Ruban, M. Dehghani, Atomic configuration and properties of austenitic steels at finite temperature: effect of longitudinal spin fluctuations, Phys. Rev. B 94 (2016): 104111, https://doi.org/10.1103/PhysRevB.94.104111.
[25] A. V Ruban, H.L. Skriver, Screened Coulomb interactions in metallic alloys. I. Universal screening in the atomic-sphere approximation, Phys. Rev. B 66 (2002): 24201, https://doi.org/10.1103/PhysRevB.66.024201.
[26] A. V Ruban, S.I. Simak, P.A. Korzhavyi, H.L. Skriver, Screened Coulomb interactions in metallic alloys. II. Screening beyond the single-site and atomic-sphere approximations, Phys. Rev. B 66 (2002): 24202, https://doi.org/10.1103/PhysRevB.66.024202.
[27] J. Kollar, L. Vitos, H.L. Skriver, From ASA towards the Full Potential, Springer-Verlag, Berlin Heidelberg New York Tokyo, 2000.
[28] H.J. Monkhorst, J.D. Pack, Special points for Brillouin-zone integrations, Phys. Rev. B 13 (1976) 5188–5192, https://doi.org/10.1103/PhysRevB.13.5188.
[29] V.L. Moruzzi, J.F. Janak, K. Schwarz, Calculated thermal properties of metals, Phys. Rev. B 37 (1988) 790–799, https://doi.org/10.1103/PhysRevB.37.790.
[30] B. Skubic, J. Hellsvik, L. Nordstrom, O. Eriksson, A method for atomistic spin dynamics simulations: implementation and examples, J. Phys. Condens. Mattter. 20 (2008): 315203, https://doi.org/10.1088/0953-8984/20/31/315203.

[31] O. Eriksson, A. Bergman, L. Bergqvist, J. Hellsvik, Atomistic Spin Dynamics, Oxford University Press, 2016. https://global.oup.com/academic/product/atomistic-spin-dynamics-9780198788669.
[32] J.M. Joubert, Crystal chemistry and Calphad modeling of the σ phase, Prog. Mater. Sci. 53 (2008) 528–583, https://doi.org/10.1016/j.pmatsci.2007.04.001.
[33] M.R. Rahul, S. Samal, G. Phanikumar, Effect of niobium addition in FeCoNiCuNbx high-entropy alloys, J. Mater. Res. 34 (2019) 700–708, https://doi.org/10.1557/jmr.2019.36.
[34] S.F. Liu, Y. Wu, H.T. Wang, J.Y. He, J.B. Liu, C.X. Chen, X.J. Liu, H. Wang, Z.P. Lu, Stacking fault energy of face-centered-cubic high entropy alloys, Intermetallics 93 (2018) 269–273, https://doi.org/10.1016/j.intermet.2017.10.004.
[35] A.J. Zaddach, C. Niu, C.C. Koch, D.L. Irving, Mechanical properties and stacking fault energies of NiFeCrCoMn high-entropy alloy, Jom 65 (2013) 1780–1789, https://doi.org/10.1007/s11837-013-0771-4.
[36] A. V Ruban, S. Shallcross, S.I. Simak, H.L. Skriver, Atomic and magnetic configurational energetics by the generalized perturbation method, Phys. Rev. B 70 (2004): 125115, https://doi.org/10.1103/PhysRevB.70.125115.
[37] A. V Ruban, S. Khmelevskyi, P. Mohn, B. Johansson, Temperature-induced longitudinal spin fluctuations in Fe and Ni, Phys. Rev. B 75 (2007): 54402, https://doi.org/10.1103/PhysRevB.75.054402.
[38] A. V Ruban, A.B. Belonoshko, N. V Skorodumova, Impact of magnetism on Fe under Earth's core conditions, Phys. Rev. B 87 (2013): 14405, https://doi.org/10.1103/PhysRevB.87.014405.
[39] R. Cardias, A. Szilva, A. Bergman, Y. Kvashnin, J. Fransson, S. Streib, A. Delin, M. I. Katsnelson, D. Thonig, A.B. Klautau, O. Eriksson, L. Nordström, Comment on "Proper and improper chiral magnetic interactions'', Phys. Rev. B 105 (2022): 26401 https://doi.org/10.1103/PhysRevB.105.026401.
[40] M. dos Santos Dias, S. Brinker, A. Lászlóffy, B. Nyári, S. Blügel, L. Szunyogh, S. Lounis, Proper and improper chiral magnetic interactions, Phys. Rev. B 103 (2021) L140408, https://doi.org/10.1103/PhysRevB.103.L140408.
[41] S. Khmelevskyi, P. Mohn, Longitudinal fluctuations of Co spin moments and their impact on the Curie temperature of the Heusler alloy Co2FeSi, J. Magn. Magn Mater. 560 (2022): 169615, https://doi.org/10.1016/j.jmmm.2022.169615.
[42] M.C. Gao, C. Zhang, P. Gao, F. Zhang, L.Z. Ouyang, M. Widom, J.A. Hawk, Thermodynamics of concentrated solid solution alloys, Curr. Opin. Solid State Mater. Sci. 21 (2017) 238–251, https://doi.org/10.1016/j.cossms.2017.08.001.